




Cite this: *RSC Adv.*, 2023, 13, 28613

# High-performance paper-based humidity sensors with Nafion/AgNWs hybrid electrodes†

Yujun Ji,‡ Gangqiang Tang,  ‡ Chun Zhao, Xin Zhao, Dong Mei, Yifan Pan and Yanjie Wang  \*

In the past decade, the development of medical health and human–computer interfaces has put forward requirements for the non-contact application of flexible electronics. Among them, flexible humidity sensors play an important role in the field of non-contact sensing by virtue of their rapid response to humidity changes. In this paper, a flexible paper-based humidity sensor with high performance was fabricated by embedded Au@AgNWs electrodes on filter paper through spraying and electroplating (EP) methods. Benefitting from the moisture-sensitive properties of the paper and the tight integration of the electrodes into the filter paper, the sensor shows the humidity monitoring range of 33–100% RH, large response value of  $I/I_0 = 1958$ , excellent linearity of  $R^2 = 0.99662$  and hysteresis performance under the low excitation voltage of only DC 1 V. In addition, the good biocompatibility of the paper-based humidity sensor endows it with multifunctional applications for breath detection, non-contact applications and food security monitoring. Easy access to raw materials and convenient preparation methods of this work provide new ideas for the development and commercialization of flexible humidity sensors.

Received 17th July 2023  
Accepted 23rd September 2023

DOI: 10.1039/d3ra04789j

rsc.li/rsc-advances

## 1. Introduction

Non-contact flexible sensors have become increasingly important in recent years, as they can effectively avoid the risk of cross-contamination compared to contact flexible sensors. In particular, the COVID-19 pandemic in the past three years has put forward wider application requirements and higher accuracy requirements for non-contact sensors.<sup>1,2</sup> Among them, the humidity sensor can detect the water molecules in the air without direct contact, which has a wide range of potential applications in medical detection,<sup>3–5</sup> e-skin,<sup>6,7</sup> etc.

The humidity sensitive layer is the core component of the humidity sensor, which determines the performance indicators of the sensor. In principle, the sensing mechanism of the most common flexible humidity sensors is based on the Grotthuss chain reaction, which is simply the process of ion migration of water molecules in the sensitive material:  $\text{H}_2\text{O} + \text{H}_3\text{O}^+ = \text{H}_3\text{O}^+ + \text{H}_2\text{O}$ .<sup>8,9</sup> The sensitive material with high hydrophilicity can adsorb mass of water molecules on its surface, resulting in more favorable ion migration to generate a humidity response signal. Therefore, the hydrophilicity of the material plays a crucial role in the humidity sensing performance. In recent years, humidity-sensing materials such as nanometallic, carbon, and polymers

have been used to prepare flexible humidity sensors. Nano-metallic materials include metal sulfides and metal oxides,<sup>10–15</sup> and carbon materials mainly include graphene oxide (GO), reduced graphene oxide (rGO),<sup>16–21</sup> which have good moisture-sensitive properties by virtue of their abundant hydrophilic functional groups on the surface and highly exposed surface area.

Compared with the above materials, polymers with super-elasticity, excellent mechanical properties and biocompatibility have attracted more attention from researchers. Polymers are divided into natural polymers such as cellulose,<sup>22</sup> protein,<sup>23</sup> etc., and synthetic polymers such as polyaniline (PANI),<sup>24</sup> polypyrrole (PPy),<sup>25</sup> polythiophene (PEDOT),<sup>26</sup> etc. Compared to synthetic polymers, natural polymeric organisms are more advantageous in terms of environmental protection and biocompatibility due to their natural degradability. Among them, cellulose is a macromolecular polysaccharide composed of glucose, which is the most widely distributed and abundant polysaccharide in nature and the most abundant natural polymer at present, with the advantages of regeneration, degradation, high thermal stability, hydrophilicity and biocompatibility. The presence of a large number of –OH groups on its polymeric linkage endows cellulose with good hydrophilicity. Paper is an industrial product made of cellulose, which often existed as a carrier of text in past times, a property that faded away with the development of information technology. Taking advantage of hygroscopic properties as well as the mature preparation process and low cost of paper, there is a huge potential application and market potential in flexible sensing applications.

Jiangsu Provincial Key Laboratory of Special Robot Technology, Hohai University, Changzhou Campus, Changzhou, 213022, China. E-mail: yjwang@hhu.edu.cn

† Electronic supplementary information (ESI) available. See DOI: <https://doi.org/10.1039/d3ra04789j>

‡ These authors contributed equally.



In 2016, F. Güder *et al.* prepared a humidity sensor with paper as a moisture-sensitive material using digitally printed graphite ink and a process cutter/printer.<sup>27</sup> Based on the hygroscopic properties of paper, changes in humidity caused by inhalation and exhalation cycles are converted into electrical signals to measure the pattern and rate of respiration. But as pointed out by George M., the electrode prepared by graphite ink is easy to crack when folded, and the voltage to excite the sensor is as high as 25 V to obtain a clear response signal, which is not conducive to subsequent acquisition system. Therefore, how to prepare a stable and high-performance electrode on the paper substrate has become the key to obtain high-performance paper-based sensors. Zhang *et al.* used pencil to draw a paper-based humidity sensor, and the conductivity of the electrode decreases to 0.5 k $\Omega$  as the number of pencil traces increases.<sup>28</sup> Zhao *et al.* similarly prepared a paper-based humidity sensor using a commercial pencil drawing electrode with oxidized multi-walled carbon nanotube (o-MWCNTs) as the sensitive layer, which exhibited good humidity monitoring range as well as stability.<sup>29</sup> However, the response performance of this sensor is affected by the bending angle of the paper.<sup>30</sup> Duan *et al.* prepared a paper-based humidity sensor rapidly using conductive tape as electrodes, and a response value of more than  $10^3$  was obtained at an excitation voltage of 10 V.<sup>31</sup> However, the poor interfaciality of the tape-paper bond limits the reduction of the sensor resistance, which increases the power consumption of the signal processing system.

Herein, a novel paper-based humidity sensor is proposed based on our group's previous research on flexible electrodes, in which the electrode is tightly embedded inside filter paper by spraying Nafion and AgNWs.<sup>32</sup> Subsequently, the oxidation resistance and firmness of AgNWs were improved by electroplating (EP). On the one hand, Nafion is used as a bonding layer to improve the adhesion between AgNWs and paper, which prevents the electrode from falling off and reduces the basic resistance of the sensor. On the other hand, Au is electroplated on AgNWs to make the bonding point between AgNWs firm, so that the basic resistance of the sensor is further reduced. The effect of structure on the sensing performance of the sensor, including the spacing of the electrodes and the pore size of the filter paper, was investigated in order to select the best combination of them for preparation. The resulting paper-based humidity sensor exhibits excellent humidity response characteristics under the low excitation voltage and multiple applications. In addition, the proposed preparing method endows the paper-based humidity sensors with high performance and large area at low cost, which is of great importance for the marketability of flexible electronic.

## 2. Experiment section

### 2.1 Materials

Nafion solution (20%) were purchased from Dupont™ (USA). AgNWs (40 nm in diameter, 20–60  $\mu$ m in length, concentration at 20 mg mL<sup>-1</sup> using ethanol as the solvent) were purchased from XFNANO Materials Tech Co., Ltd (Nanjing, China). EtOH (99.5%) and *N,N*-dimethylacetamide (DMAC) (99%) were

purchased from Aladdin Co., Ltd (Shanghai, China). Filter paper was purchased from Jiesiman Co., Ltd (Wuhan, China). Auxiliary reagents including MgCl<sub>2</sub>, K<sub>2</sub>CO<sub>3</sub>, NaBr, NaCl, KCl and allochroic silicagel were obtained from J&K Chemical Inc. (Beijing, China). All the reagents were used as received without further purification.

### 2.2 Preparation of the solutions

DMAC was used as a solvent to dilute the Nafion solution in order to disperse the solution uniformly and to prevent the spraying gun from clogging. As shown in Fig. 1a, 1 ml of Nafion solution was mixed with 5 ml of DMAC, stirred magnetically for 30 min at 500 rpm, and then put into an ultrasonic shaker for 30 min to obtain a well-dispersed Nafion/DMAC solution. Similarly, EtOH was used as a solvent to dissolve the AgNWs solution. Take 1 ml of AgNWs mixed with 50 ml of EtOH and put it into the ultrasonic shaker for 30 min. It should be noted that the temperature is set to 25 °C to prevent solvent evaporation.

### 2.3 Process of spraying

According to the electrode design, a mask-plate with two square cutouts is placed on top of the paper, and the cutouts are used to control the size of the spray electrode. The distance between the two electrodes can be controlled by changing the size of the middle beam. In this paper, additional mask-plates with different sizes (2 mm, 3 mm) of the middle beam were designed to test the effect of electrode interval on the performance of the humidity sensor. In order to make the AgNWs firmly embedded in the filter paper, the spraying process is divided into two steps. As shown in Fig. 1a, 0.4 ml Nafion/DMAC solution was sprayed on the paper repeatedly covered the paper with a mask-plate *via* a manual spray pen (nozzle diameter: 0.3 mm, air pressure: 0.4 MPa), and get a uniform adhesion layer after the DMAC volatilizes. Take 1 ml of the AgNWs/EtOH solution after oscillation to a manual spray pen, continue to spray the solution on the paper sprayed with the adhesion layer, and obtain a uniform AgNWs electrode after the alcohol is volatilized. Since the EtOH can dissolve the Nafion and evaporate rapidly, it makes the AgNWs in the solvent firmly embedded in the Nafion.<sup>33</sup>

### 2.4 Process of EP

As shown in Fig. 1b, DC regulated power supply is set to 5 V. The positive electrode is connected with the titanium mesh and put into the gold plating water. The AgNWs electrode was held by metal tweezers and immersed in gold water for 90 s until the surface of electrodes turns golden. The gold ions in the gold water were reduced to gold atoms and deposited on the AgNWs through electrochemical method. The antioxidant properties of the electrodes were further enhanced due to the weaker chemical activity possessed by the gold elements. The electroplated prototype was finally trimmed at the edges to obtain the dimensions and structure as shown in Fig. 1c. The electrodes and the electrochemical workstation were connected with conductive adhesive tape as shown in Fig. S1.†



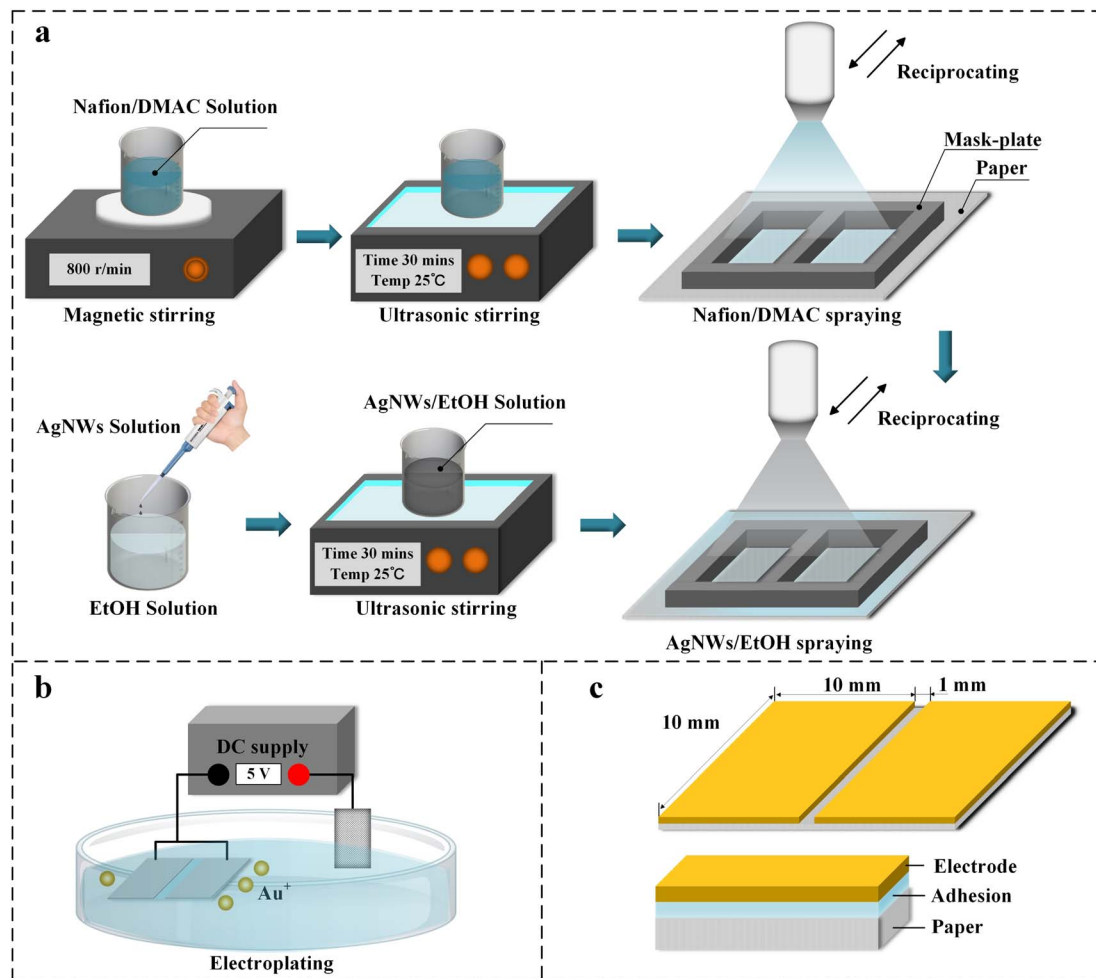


Fig. 1 The process of preparing the paper-based humidity sensors. (a) Preparation of the solution and process of spraying. (b) Process of electroplating (EP). (c) Schematic structure of the prepared sample.

## 2.5 Characterization and measurement

The microstructure of the humidity sensor was characterized via a ZEISS Sigma 500 field emission scanning electron microscope. The images were captured by a digital camera (XIAOMI 10S). And the microscopic images were captured by an optical microscope (PMS-XHD-AF03). The resistance of the sample was measured by a Jingge Electronics Co., Ltd. M3 four-probe meter (Suzhou, China). The raw paper as well as the paper processed with Au@AgNWs electrodes were prepared for the composition of the sensor via X-ray diffraction (XRD) and energy-dispersive X-ray spectroscopy (EDS) analysis. XRD analysis was measured via X-ray diffractometer (Rigaku ULTIMA IV) with scanning range  $10^\circ$  to  $80^\circ$  at a rate of  $10^\circ$  per minute. EDS analysis was measured by an Extreme-resolution Analytical Field Emission SEM using Oxford Nordly Max3 as the detector. Different humidity environments were obtained from equilibrium states of different saturated salt solutions at  $25^\circ\text{C}$ . As shown in Fig. S1,<sup>†</sup> 33% RH, 43% RH, 57% RH, 75% RH and 84% RH humidity atmospheres were obtained by deploying saturated  $\text{MgCl}_2$ ,  $\text{K}_2\text{CO}_3$ ,  $\text{NaBr}$ ,  $\text{NaCl}$ , and  $\text{KCl}$  solutions in the closed glass vials, respectively. Nearly 0% RH was obtained by placing

allochroic silicagel in a closed glass bottle. And nearly 100% RH was obtained in a closed glass bottle by filling it with deionized water. The humidity response curve is obtained by switching the sample between different humidity environments. The amperometric  $I$ - $T$  curve module in the electrochemical workstation (CHI660E) was used for the humidity response test, set with the DC excitation voltage of 1 V and a sampling frequency of 0.1 s. The cyclic voltammetry module in the electrochemical workstation (CHI660E) was also selected for testing the electrochemical performance of the sensor, setting the scan rate to  $0.1\text{ V s}^{-1}$  from  $-1\text{ V}$  to  $1\text{ V}$ .

## 3. Results and discussions

Fig. 2a shows the macroscopic morphology of the prepared sensor before and after EP step, where two  $10\text{ mm} \times 10\text{ mm}$  square electrodes are formed on the paper surface after spraying. Subsequently, the electrodes were transformed from silver to gold by plating AgNWs, indicating that the gold was fully attached to the AgNWs. Fig. 2b shows an interval of 1 mm between the two electrodes. The edges of the electrodes appear





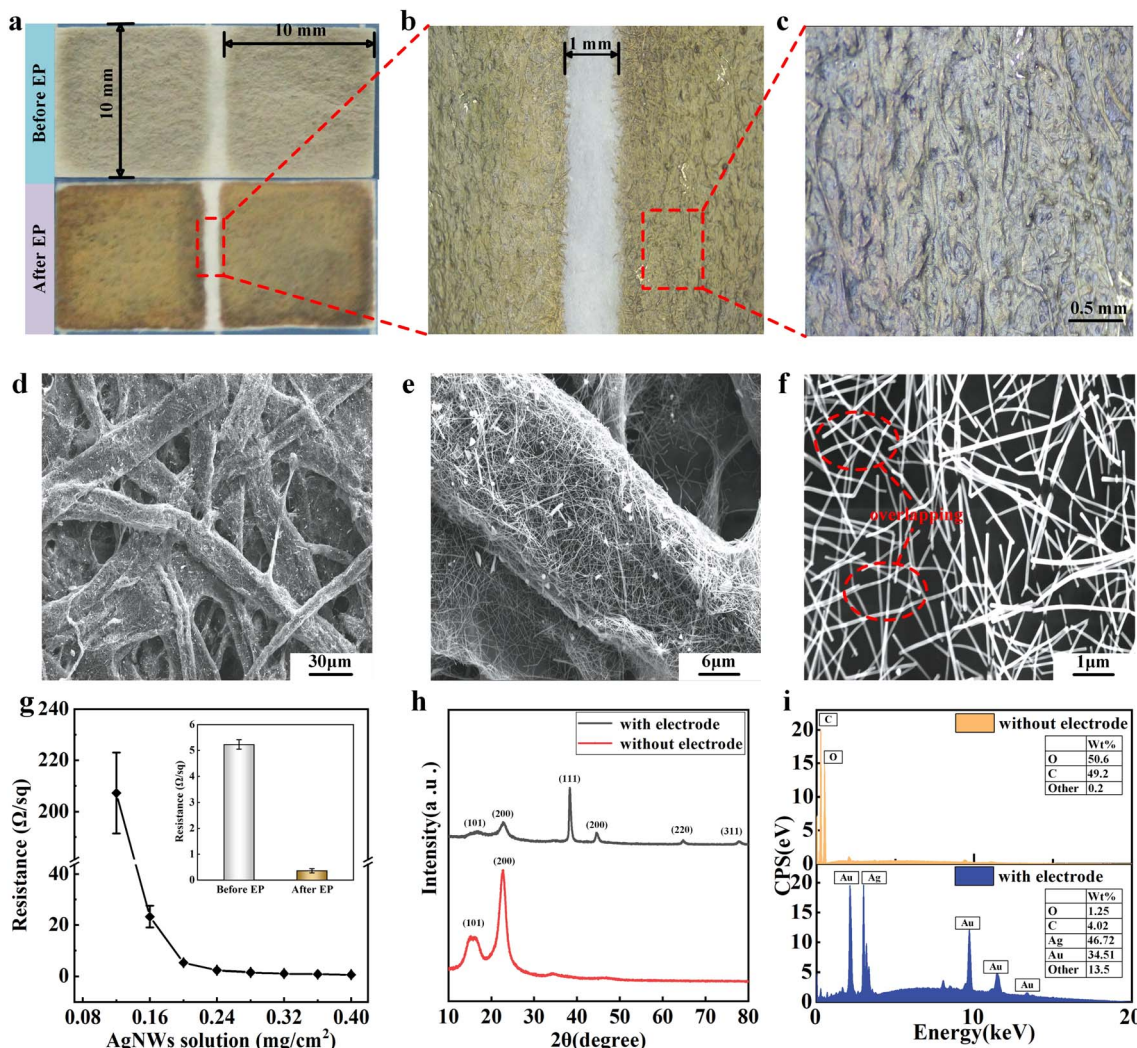


Fig. 2 The surface dimensions of the paper-based humidity sensors captured by (a) the camera and (b and c) optical microscope. (d–f) Surface SEM image of the electrodes of the sensors. (g) Relationship between AgNWs of different densities and surface resistance of electrodes. The inset shows the surface resistance before and after EP. (h) XRD and (i) EDS analysis of raw paper without electrodes and sensors with electrodes.

well parallel under the beam of the mask-plate, so the spacing is considered to be uniform. To further demonstrate the surface morphology of the electrodes, the Au@AgNWs bonded well with the surface of the paper without defects such as voids and cracks as shown in Fig. 2c.

Fig. 2d–f displays cross-sectional scanning electron microscopy (SEM) images of the humidity sensor to demonstrate the combination of electrodes and paper. As shown in Fig. 2d and e, the paper shows a typical cellulose mesh structure in microscopic view. AgNWs are densely deposited on the surface of the cellulose and are present even in the defects of the cellulose, which is favorable to the conductivity and stability of the sensor. It can be observed that the AgNWs vary in brightness at the intersections in Fig. 2f, indicating that the AgNWs overlap each other, resulting in an improvement in the stability and conductivity of the electrodes.

The prepared samples were dried for 24 hours and subsequently subjected to cyclic voltammetry tests in a dry

environment to show that the materials undergo no irreversible reactions when energized. It can be seen from Fig. S2† that the curve has no obvious redox peaks and is symmetrical up and down, which indicates that no redox reaction is occurring in the material during the forward and reverse sweeps, and no irreversible reaction is occurring at the operating voltage. Moreover, the sensor's performance is affected by the electrode resistance. Therefore, the relationship between the AgNWs density and the electrode surface resistance was investigated by spraying different contents of AgNWs solution on a substrate with an area of 1 cm<sup>2</sup>. As shown in Fig. 2g, the electrode surface resistance firstly shows a precipitous decrease as the silver nanowire density increases under unit area. When the density of sprayed AgNWs reached 0.2 mg cm<sup>−2</sup>, the surface resistance of the electrode drops to below 10 Ω. Then the resistance decreases slowly with the increase of spraying volume. The reason for this phenomenon is that AgNWs are first embedded in the adhesion layer and are not connected to each other.



When the density is increased, the AgNWs are exposed on the surface of the substrate layer and overlap with each other, so that the resistance drops suddenly. Therefore, we chose the AgNWs concentration of  $0.2 \text{ mg cm}^{-2}$  as the standard in the subsequent study. Silver has a very large contact area with air in the nano-state, which is very easy to be oxidized and lose conductivity. Therefore, we use EP method to enhance the oxidation resistance of the electrode because the chemical activity of gold is weaker than that of silver. Moreover, EP can increase the electrical conductivity and firmness due to gold atoms attached on top of the AgNWs increased the contact area of the lapped electrodes. As shown in the inset of Fig. 2g, the surface resistance is further reduced to below  $1 \Omega$ .

In order to analyze the composition of the sensors, the raw paper as well as the paper processed with Au@AgNWs electrodes were analyzed by X-ray diffraction (XRD) and energy dispersive X-ray spectroscopy (EDS). As shown in Fig. 2h, the XRD analysis of raw paper without electrodes showed two distinct characteristic peaks at  $16.5^\circ$  and  $22.5^\circ$ . These peaks corresponded to the diffraction of cellulose along the (101) and (002) planes, which suggests that the paper is partially made of cellulose.<sup>34</sup> In contrast, the XRD analysis of the paper with electrodes yielded multiple characteristic peaks at  $38.2^\circ$  (111),  $44.6^\circ$  (200),  $64.6^\circ$  (220), and  $77.5^\circ$  (311), which corresponded to the characteristics of Au/Ag.<sup>35–38</sup> Additionally, the intensity of the characteristic peaks for cellulose decreased, indicating that the paper was covered by the Au@AgNWs electrodes. EDS energy spectrum analysis can also verify the aforementioned results in the Fig. 2i. Excluding the H element, which is not detectable by EDS analysis, the paper is initially composed of 50.6% C and 49.2% O, corresponding to the composition of cellulose. After electrode processing, the detected composition contained 46.72% Ag and 34.51% Au, indicating successful adhesion of Au@AgNWs to the paper. Combining the SEM images shown in Fig. 2d–f and the compositional analysis shown in Fig. 2h–i, it can be concluded that the sensor consists of cellulose with micrometer diameter and Au@AgNW with nanometer diameter. The cellulose that makes up paper acts as a moisture-sensitive material capable of absorbing water molecules in the air, producing a humidity-sensing signal. The Au@AgNWs electrodes firmly attached to the paper are capable of transmitting electrical signals to the detection system.

Fig. 3a illustrates the tight attachment of the electrode layer with the filter paper through the Nafion bonding layer. Nafion covers the cellulose of the paper, where the AgNWs are tightly embedded. The exposed part of the AgNWs is wrapped by gold atoms, which improves the adhesion strength of the electrode. Fig. S3† demonstrates the effect of the above process on electrode adhesion through tape adhesion tests.

The sensing mechanism of the sensor is shown in Fig. 3b–d. An interval was left between the two electrodes so that the electrodes not conductive under normal conditions. When the relative humidity of the air around the sensor increases, cellulose contains abundant hydrophilic –OH groups to adsorb water molecules in the air as shown in Fig. 3b. According to the previous report,<sup>31</sup> the oxygen atoms in the water molecules form hydrogen bonds with the hydrogen atoms of –OH. Initially,

a continuous and organized water film is formed on the surface of the cellulose. Subsequently, as water molecules continue to be absorbed, a second water film is formed on the initial one that is more freely arranged as shown in Fig. 3c. This free water film enables carriers to move, causing a drop in conductivity. As the humidity increases, water molecules produce  $\text{H}_3\text{O}^+$  and  $\text{OH}^-$  ions on the liquid water film. The ions are able to move directionally after applying voltage through the electrodes, resulting in increased conductivity between the electrodes. Thus paper-based humidity sensors have a large response in high humidity conditions. On the contrary, at low humidity it is not only difficult for water molecules to form a continuous water film but also only a few  $\text{OH}^-$  and  $\text{H}^+$  ions migrate as carriers, resulting in low response values for paper-based humidity sensors.

In order to obtain a humidity sensor with optimal performance, we explored the influence of preparation factors on the sensor performance. The interval of electrodes is one of the important parameters affecting the performance of paper-based humidity sensors. As shown in Fig. 4a and b, the humidity corresponding curves at different humidity levels were tested for the sensors based on medium filter paper with different intervals of 1 mm, 2 mm and 3 mm. As the electrode interval increases, the humidity response value appears to be attenuated, while the detection range of the sensor is reduced. It should be noted that the excitation voltage of the humidity response test in this paper is DC 1 V. This is due to the fact that the increase in electrode interval causes the paper surface to absorb more water molecules in order to form a continuous water film. Considering the accuracy of spraying process and 3D printing, a paper-based humidity sensor with 1 mm electrode interval was chosen in the follow-up experiments. The pore size of the filter paper is another important parameter affecting the sensing performance of paper-based humidity sensor. The fast, medium and slow filter papers with pore sizes of 10 microns, 5 microns and 3 microns respectively were selected to conduct experiments. The larger pore size means the larger contact area between the paper surface and air, the more –OH functional groups can combine with water molecules, which benefits to improve the moisture-sensitive properties of the paper. As shown in Fig. 4c and d, the response values of fast filter paper with large pore size are greater than those of medium and slow filter paper with smaller pore sizes at each humidity level, which is consistent with the theoretical analysis. Therefore, fast filter paper with an interval of 1 mm was identified as the sample with the best humidity response performance.

After determining the optimal parameters of the preparation process, the humidity sensing performance of the sample with the best sensing performance (fast filter paper with an interval of 1 mm) was characterized. Fig. 5 shows the humidity sensing characteristics of the paper-based humidity sensor with fast filter paper as substrate and electrode interval of 1 mm. The sensor was placed in a glass bottle at 0% RH for 20 minutes to dry completely, then it was put in a glass bottle at 100% RH for 650 s to absorb and translated in a glass bottle at 0% RH for 400 s to desorb, and the cycle was repeated five times. The Fig. 5a shows the response recovery curve for five consecutive

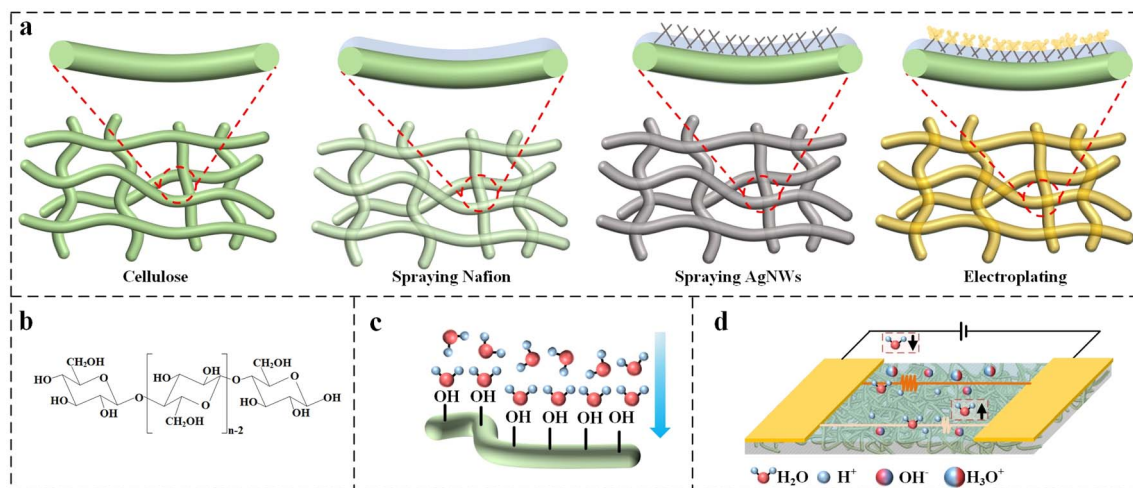


Fig. 3 (a) Schematic diagram of electrode adhesion to the paper. (b) Molecular formula of cellulose. (c) Schematic diagram of absorption of water molecules by  $-OH$ . (d) Schematic diagram of the sensing mechanism.

switches between high and low humidity, indicating good cyclic stability of the sensor. To clearly present the response time and recovery time, the single response recovery cycle curve after zooming in is shown in Fig. 5b. The response time and recovery time in logarithmic coordinates are calculated to be 528 s and 237 s, respectively. The slower response recovery speed is a result of the material properties of the filter paper, which is a common problem for paper-based humidity sensors (Table 1).

According to the sensing mechanism described above, the increase in conductivity of paper during the moisture absorption process requires the formation of a water film in which the carriers can move freely, but this water film disappears first during the moisture removal process. Therefore, the response time of the sensor is slower than the recovery time. Fig. 5c shows the response curves of the sensor in logarithmic coordinates for different humidity variation ranges. Referring to

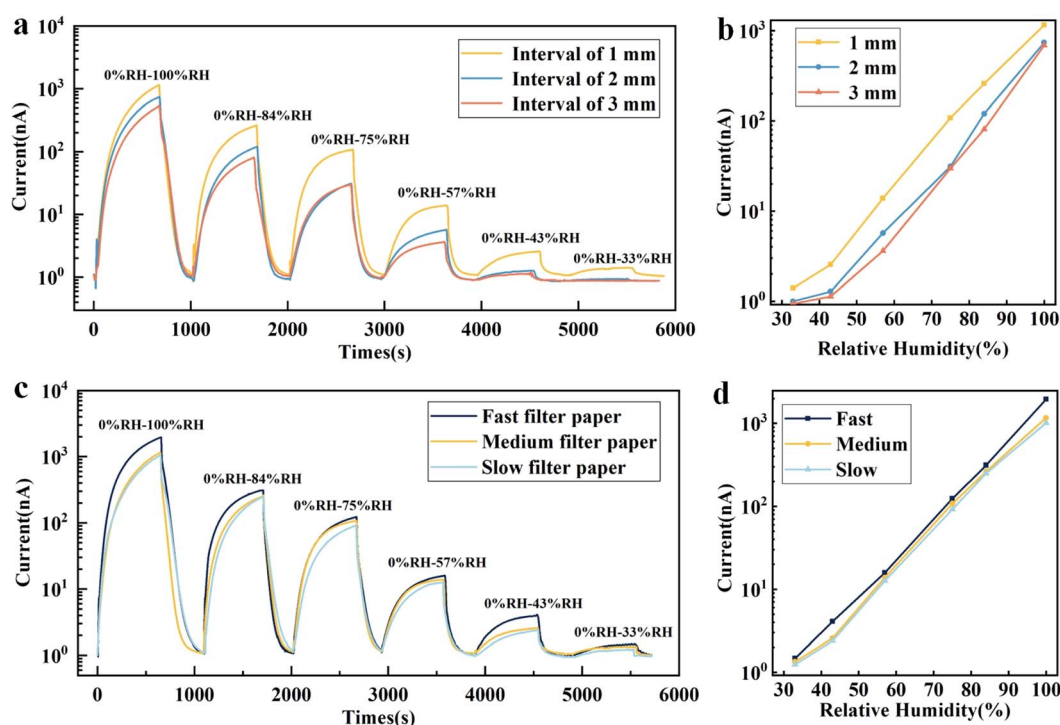


Fig. 4 Humidity sensing response of sensors based on electrodes with different interval and paper with different pore sizes. (a) Dynamic humidity response of the sensor with different interval between electrodes to 33%, 54%, 75%, 84% RH, and 100% RH (from 0% RH), respectively. (b) Relationship between sensor response values for different electrode intervals and different relative humidity. (c) Dynamic sensing response and (d) response-RH relationship of sensors based on different types of filter paper.





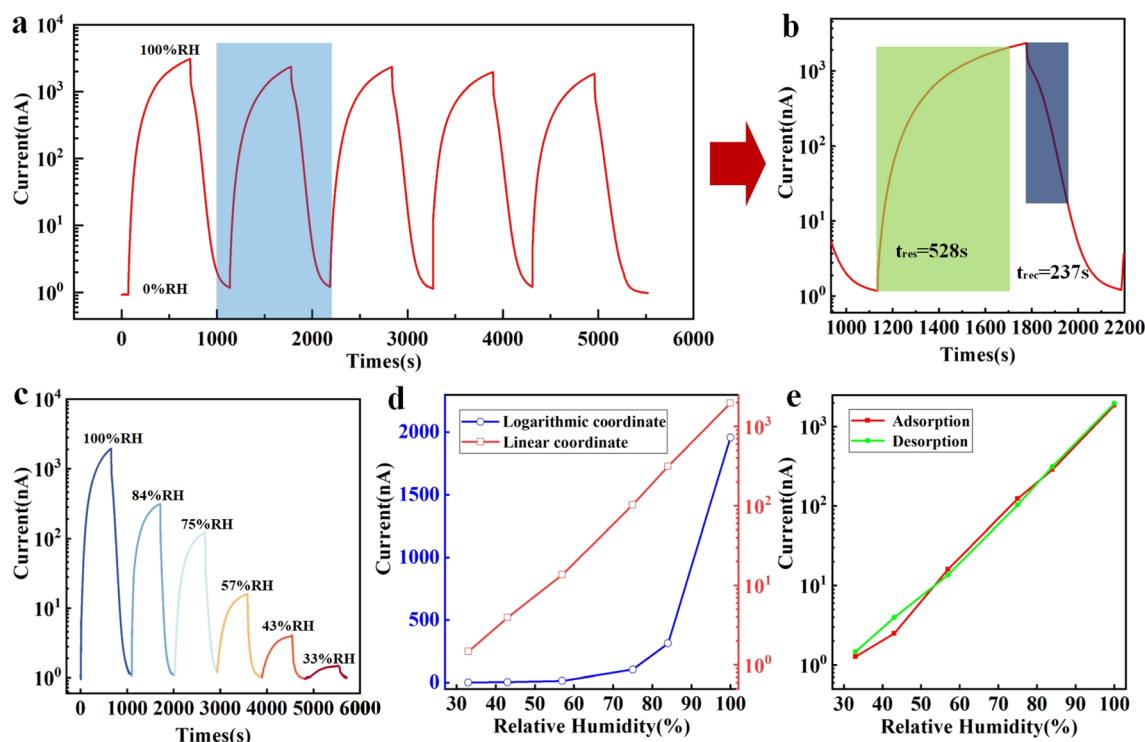


Fig. 5 Humidity-sensing properties of the humidity sensor. (a) Response and recovery curves for five cycles from 0% RH to 100% RH. (b) Amplified response and recovery curve. (c) Dynamic response characteristics curve of humidity sensor from 0% RH to 100%, 84%, 75%, 57%, 43%, 33% RH. (d) Current–RH curves in logarithmic and linear coordinates. (e) Humidity response in adsorption and desorption state.

Fig. 5d, it can be seen that the sensor shows a nonlinear response in linear coordinates, with a low response signal in low humidity environments (below 57% RH) and a large response signal in high humidity environments (above 57%). With suitable data processing and linear fitting as shown in Fig. S4,† it can be seen in logarithmic coordinates that the humidity sensor has a good linear response in the humidity range of 33–100% RH, with a response value of up to 1958 ( $I/I_0$ ) at an excitation voltage of DC 1 V only, where  $I$  means the response value in 100% RH and  $I_0$  means the response value in 0% RH. The hysteresis of the humidity sensor usually refers to the difference between the response signals of the sensor in the process of moisture absorption and desorption. The moisture absorption and desorption curves of the sensor are obtained by changing the order of the humidity environment (from low to high sequentially and from high to low sequentially). As shown in Fig. 5e, it can be seen that they are almost identical, indicating that the sensor has a high stability. The durability of the

sensor relies on the paper quality. When left in the air for extended periods of time, the paper oxidizes, leading to a short shelf life for the sensor device. Nonetheless, our sensor demonstrates a good response stability over an extended period (6000 s), as illustrated in Fig. S5.† Low cost and fast preparation are significant benefits of the paper-based sensor technology, notwithstanding the short durability of the device.

Benefiting from the large response values of paper-based humidity sensors under high humidity conditions, we predict that they can be used in daily life for breath detection. As shown in Fig. S6,† the sensor is installed in the mask to detect the breathing of a volunteer who is 28 years old and healthy. When a volunteer exhales, the exhaled gas is sufficiently humidified to fill the surface of the sensor with water molecules, causing the conductivity to rise. Conversely, during inhalation, the humid gas around the sensor is drawn into the body, causing its conductivity to drop. The respiratory response signals in sleeping and after sporting are shown in Fig. 6a and b. The

Table 1 Comparison on the performance of various paper-based humidity sensors

Materials	Output	RH range (%)	Response	Response/recovery	Ref
o-MWCNTs	Current	33–95	18–33% ( $\Delta I/I_0$ )	5–8 min/7–11 min	29
Paper	Current	41.1–91.5	1647 ( $I/I_0$ )	472 s/19 s	31
ZnO	Resistance	20–70	$\sim 14$ ( $R_0/R$ )	1 min/2–10 min	39
Paper	Voltage	41.1–91.5	$\sim 81.4$ ( $V/V_0$ )	109 s/113 s	40
ZnS : Cu	Current	20–90	6.50 $\mu A/RH$	3 min/2.4 min	41
Paper	Current	33–100	1958 ( $I/I_0$ )	528 s/237 s	This work

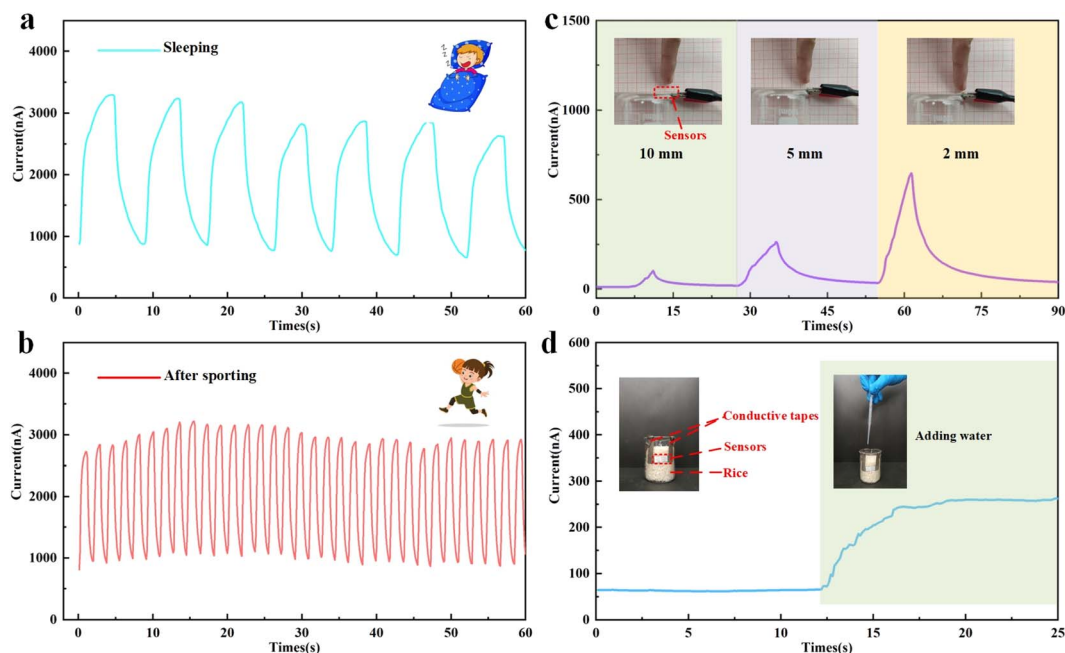


Fig. 6 Current response curve of the volunteer breathing (a) during sleep. (b) After sporting. (c) Current response curve when the finger is 10 mm, 5 mm and 2 mm away from the sensor. (d) Current curve of the sensor before and after rice wetting.

response signal of the sensor is consistent with the respiratory frequency, whether in motion with a fast respiratory rate or in sleep with a slow respiratory rate. And there is a clear process of moisture absorption and dehumidification, which proves that the sensor meets the needs of respiratory detection.

To investigate the potential application of humidity sensors in non-contact electronics, non-contact skin humidity response experiments were conducted. The sensor was placed on a horizontal surface and the sensor electrodes were connected to the signal acquisition platform by wire clamping. Since the human skin surface is constantly evaporating sweat, a relatively weak response signal appears when the finger is 10 mm away from the sensor. As shown in Fig. 6c, when the finger is closer to the sensor, the larger the signal generated. It proves that the sensor has application value in the field of non-contact electronics.

In addition, humidity is a very important indicator in food storage, as food is prone to spoilage and deterioration at high humidity levels. Benefiting from the high sensitivity of the paper-based sensor, it has potential applications in food security. As shown in Fig. 6d, the sensor is buried in ordinary rice and the electrodes are led through adhesive conductive tapes. Under normal conditions, the rice is extremely absorbent, keeping the area around the sensor dry. When water is added into the rice, the sensing immediately showed a response signal, indicating that the sensor sensed that the surrounding rice had been moistened. This indicates that the sensor can be applied to grain bin moisture monitoring.

## 4. Conclusions

In this work, a facile method was proposed to prepare paper-based humidity sensors, and Au@AgNWs embedded in

Nafion adhesion layer were used as electrodes with interval of 1 mm while fast filter paper with large pore size was used as substrate and humidity sensitive material. According to humidity measurement, the sensor exhibits the advantages of large response value of  $I/I_0 = 1958$  from 33% RH to 100% RH, excellent linearity of  $R^2 = 0.99662$ , hysteresis performance and stability under the low excitation voltage of only DC 1 V. The excellent humidity response allows the paper-based humidity sensor to distinguish between different frequencies of breathing. In addition, the signal response generated to the approach and the distance of a finger verified the non-contact application. The high sensitivity of paper-based sensors endows them with potential application value for grain storage.

The main advantages of the paper-based humidity sensor are as follows: (i) the simple and low-cost preparation method of humidity sensor provides a new idea for the development of non-contact flexible electronic. (ii) The close combination of the electrode and the substrate reduces the resistance of the sensor, resulting in a signal response of more than  $10^3$  with only DC 1 V, which effectively reduces the power consumption and design cost of the signal processing system.

## Author contributions

Yujun Ji: conceptualization, methodology, software, validation, formal analysis, data curation, writing – original draft. Gang-qiang Tang: conceptualization, methodology, data curation, writing – review & editing. Chun Zhao: methodology, technical support. Xin Zhao: methodology, writing – review & editing, drawings. Dong Mei: supervision, software. Yifan Pan: supervision, software. Yanjie Wang: supervision, project administration, funding acquisition.





## Conflicts of interest

There are no conflicts to declare.

## Acknowledgements

This research was supported by the Fundamental Research Funds for the Central Universities (B230202011), the National Natural Science Foundation of China (51975184), the National Key Research and Development Program of China (2019YFB1311600). The authors gratefully acknowledge the supports.

## References

- 1 H. Jeong, J. Y. Lee, K. H. Lee, *et al.*, Differential cardiopulmonary monitoring system for artifact-canceled physiological tracking of athletes, workers, and COVID-19 patients, *Sci. Adv.*, 2021, 7(20), eabg3092.
- 2 G. Quer, J. M. Radin, M. Gadaleta, *et al.*, Wearable sensor data and self-reported symptoms for COVID-19 detection, *Nat. Med.*, 2021, 27(1), 73–77.
- 3 A. Ullah, M. H. Zulfiqar, M. A. Khan, M. Zubair, M. Q. Mehmood and Y. Massoud, Fast Response Facile Fabricated IDE-Based Ultra-sensitive Humidity Sensor for Medical Applications, *ACS Omega*, 2023, 8(19), 16842–16850.
- 4 S. Zou, L. Q. Tao, G. Wang, *et al.*, Humidity-Based Human-Machine Interaction System for Healthcare Applications, *ACS Appl. Mater. Interfaces*, 2022, 14(10), 12606–12616.
- 5 L. Hou, Y. Li, Y. Fu, *et al.*, Ultra-sensitive optical fiber humidity sensor *via* Au-film-assisted polyvinyl alcohol micro-cavity and Vernier effect, *IEEE Trans. Instrum. Meas.*, 2022, 71, 1–9.
- 6 F. Yin, Y. Guo, Z. Qiu, *et al.*, Hybrid electronic skin combining triboelectric nanogenerator and humidity sensor for contact and non-contact sensing, *Nano Energy*, 2022, 101, 107541.
- 7 W. Xiong, H. Feng, H. Liwang, D. Li, W. Yao, D. Duolikun, Y. Zhou and Y. Huang, Multifunctional Tactile Feedbacks Towards Compliant Robot Manipulations *via* 3D-Shaped Electronic Skin, *IEEE Sens. J.*, 2022, 22(9), 9046–9056.
- 8 Y. Lu, G. Yang, Y. Shen, *et al.*, Multifunctional flexible humidity sensor systems towards noncontact wearable electronics, *Nano-Micro Lett.*, 2022, 14(1), 150.
- 9 D. Zhang, Z. Xu, Z. Yang, *et al.*, High-performance flexible self-powered tin disulfide nanoflowers/reduced graphene oxide nanohybrid-based humidity sensor driven by triboelectric nanogenerator, *Nano Energy*, 2020, 67, 104251.
- 10 V. Jagadeesha Angadi, K. M. Batoo, S. Hussain, S. O. Manjunatha, S. Wang and S. P. Kubrin, Synthesis and study of transition metal (Co, Cu, and Ni) substituted ferrites for humidity sensor applications, *J. Mater. Sci.: Mater. Electron.*, 2023, 34, 301.
- 11 M. R. Adib, Y. Lee, V. V. Kondalkar, *et al.*, A highly sensitive and stable rGO: MoS<sub>2</sub>-based chemiresistive humidity sensor directly insertable to transformer insulating oil analyzed by customized electronic sensor interface, *ACS Sens.*, 2021, 6(3), 1012–1021.
- 12 N. Li, Y. Jiang, C. Zhou, *et al.*, High-performance humidity sensor based on urchin-like composite of Ti<sub>3</sub>C<sub>2</sub> MXene-derived TiO<sub>2</sub> nanowires, *ACS Appl. Mater. Interfaces*, 2019, 11(41), 38116–38125.
- 13 R. Nitta, H. E. Lin, Y. Kubota, *et al.*, CuO nanostructure-based flexible humidity sensors fabricated on PET substrates by spin-spray method, *Appl. Surf. Sci.*, 2022, 572, 151352.
- 14 P. Wang, H. Ding, X. Li, Y. Liu, Y. Sun, Y. Li, G. Xu, S. Chen and X. Wang, Stretchable and Self-Adhesive Humidity-Sensing Patch for Multiplexed Non-Contact Sensing, *ACS Appl. Mater. Interfaces*, 2023, 15(32), 38562–38571.
- 15 S. Yu, C. Chen, H. Zhang, *et al.*, Design of high sensitivity graphite carbon nitride/zinc oxide humidity sensor for breath detection, *Sens. Actuators, B*, 2021, 332, 129536.
- 16 D. Lei, Q. Zhang, N. Liu, *et al.*, Self-powered graphene oxide humidity sensor based on potentiometric humidity transduction mechanism, *Adv. Funct. Mater.*, 2022, 32(10), 2107330.
- 17 Y. Yu, G. He, X. Zhu, J. Yu, Y. Shi, Y. Lei and F. Sun, A flexible humidity sensor constructed by ordered-pore-array of slightly reduced graphene oxide with much enhanced sensing response, *Surf. Interfaces*, 2023, 41, 103204.
- 18 W. Noh, Y. Go and H. An, Reduced Graphene Oxide/ Polyelectrolyte Multilayers for Fast Resistive Humidity Sensing, *Sensors*, 2023, 23(4), 1977.
- 19 V. J. Angadi, B. Chethan, V. Pattar, N. B. Shighalli, S. A. Patil, M. Ubaidullah, S. S. Sehgal, C. Prakash, S. O. Manjunatha and K. Manjunatha, Graphene-Cobalt chromate ceramics composite for humidity sensor Applications, *J. Alloys Compd.*, 2023, 947, 169438.
- 20 L. Lan, X. Le, H. Dong, *et al.*, One-step and large-scale fabrication of flexible and wearable humidity sensor based on laser-induced graphene for real-time tracking of plant transpiration at bio-interface, *Biosens. Bioelectron.*, 2020, 165, 112360.
- 21 H. Cho, C. Lee, C. Lee, S. Lee and S. Kim, Robust, Ultrathin, and Highly Sensitive Reduced Graphene Oxide/Silk Fibroin Wearable Sensors Responded to Temperature and Humidity for Physiological Detection, *Biomacromolecules*, 2023, 24(6), 2606–2617.
- 22 J. Yu, Y. Feng, D. Sun, *et al.*, Highly conductive and mechanically robust cellulose nanocomposite hydrogels with antifreezing and antidehydration performances for flexible humidity sensors, *ACS Appl. Mater. Interfaces*, 2022, 14(8), 10886–10897.
- 23 Y. Zheng, L. Wang, L. Zhao, *et al.*, A flexible humidity sensor based on natural biocompatible silk fibroin films, *Adv. Mater. Technol.*, 2021, 6(1), 2001053.
- 24 D. Y. Imali, E. C. J. Perera, M. N. Kaumal and D. P. Dissanayake, Fabrication and characterization of a flexible and disposable impedance-type humidity sensor based on polyaniline (PANI), *RSC Adv.*, 2023, 13(10), 6396–6411.



- 25 X. Liu, D. Zhang, D. Wang, *et al.*, A humidity sensing and respiratory monitoring system constructed from quartz crystal microbalance sensors based on a chitosan/polypyrrole composite film, *J. Mater. Chem. A*, 2021, **9**(25), 14524–14533.
- 26 M. I. Abdullah, A. R. Ahmad and A. F. Abdulameer, Fabrication and Characterization of Humidity Sensors Based on PEDOT: PSS Doped with Gold and Silver Nanoparticles by Laser Ablation, *Int. J. Nanosci.*, 2023, 2350038.
- 27 F. Güder, A. Ainla, J. Redston, *et al.*, Paper-based electrical respiration sensor, *Angew. Chem., Int. Ed.*, 2016, **55**(19), 5727–5732.
- 28 Y. Zhang, Z. Duan, H. Zou, *et al.*, Drawn a facile sensor: a fast response humidity sensor based on pencil-trace, *Sens. Actuators, B*, 2018, **261**, 345–353.
- 29 H. Zhao, T. Zhang, R. Qi, *et al.*, Drawn on paper: a reproducible humidity sensitive device by handwriting, *ACS Appl. Mater. Interfaces*, 2017, **9**(33), 28002–28009.
- 30 N. I. Sonil, Z. Ullah, J. Chen and G. P. Wang, Wearable strain sensors for human motion detection and health monitoring based on hybrid graphite-textile flexible electrodes, *J. Mater. Res. Technol.*, 2023, **26**, 764–774.
- 31 Z. Duan, Y. Jiang, M. Yan, *et al.*, Facile, flexible, cost-saving, and environment-friendly paper-based humidity sensor for multifunctional applications, *ACS Appl. Mater. Interfaces*, 2019, **11**(24), 21840–21849.
- 32 C. Zhao, Y. Wang, G. Tang, *et al.*, Biological Hair-Inspired AgNWs@ Au-Embedded Nafion Electrodes with High Stability for Self-Powered Ionic Flexible Sensors, *ACS Appl. Mater. Interfaces*, 2022, **14**(40), 46023–46031.
- 33 C. Zhao, Y. Ji, G. Tang, *et al.*, Rapid Preparation of Novel Ionic Polymer–Metal Composite for Improving Humidity Sensing Effect, *Polymers*, 2023, **15**(3), 733.
- 34 H. Bian, Y. Yang, P. Tu and J. Y. Chen, Value-Added Utilization of Wheat Straw: From Cellulose and Cellulose Nanofiber to All-Cellulose Nanocomposite Film, *Membranes*, 2022, **12**(5), 475.
- 35 S. Deng, B. Zhao, Y. Xing, Y. Shi, Y. Fu and Z. Liu, Green synthesis of proanthocyanidins-functionalized Au/Ag bimetallic nanoparticles, *Green Chem. Lett. Rev.*, 2020, **14**(1), 45–50.
- 36 J. Ji, Z. Li, W. Sun and H. Wang, Thermal annealing induced tunable localized surface plasmon resonance of Au/Ag bimetallic thin film, *Chem. Phys.*, 2021, **541**, 111034.
- 37 S. Fahad, H. Yu, L. Wang, Y. Wang, T. Lin, B. U. Amin, K.-U.-R. Naveed, R. U. Khan, S. Mehmood, F. Haq, Y. Xing and M. Usman, Synthesis of AgNWs Using High Molecular Weight PVP As a Capping Agent and Their Application in Conductive Thin Films, *J. Electron. Mater.*, 2021, **50**(5), 2789–2799.
- 38 Z. Zhang, C. Chen, G. Liu, C. Li, S. Kurosaka, S. Nagao and K. Suganuma, Enhancement of bonding strength in Ag sinter joining on Au surface finished substrate by increasing Au grain-size, *Appl. Surf. Sci.*, 2019, **485**, 468–475.
- 39 G. Niarchos, G. Dubourg, G. Afroudakis, M. Georgopoulos, V. Tsouti, E. Makarona, V. Crnojevic-Bengin and C. Tsamis, Humidity sensing properties of paper substrates and their passivation with zno nanoparticles for sensor applications, *Sensors*, 2017, **17**(3), 516.
- 40 Z. Duan, Z. Yuan, Y. Jiang, Q. Zhao, Q. Huang, Y. Zhang, B. Liu and H. Tai, Power generation humidity sensor based on primary battery structure, *Chem. Eng. J.*, 2022, **446**, 136910.
- 41 Y. He, M. Zhang, N. Zhang, D. Zhu, C. Huang, L. Kang, X. Zhou, M. Hu and J. Zhang, Paper-Based ZnS: Cu Alternating Current Electroluminescent Devices for Current Humidity Sensors with High-Linearity and Flexibility, *Sensors*, 2019, **19**(21), 4607.

